J Mater Sci (2025) 60:23463–23479

Composites & nanocomposites

Interfacial charge transfer in graphene–$ZnFe_2O_4$ thin films for efficient photocatalytic degradation of antibiotics under visible light

Fatma Ezzahra Dhif[1,*], Neila Jebbari[1], Alberto Vomiero[2,3], Elisa Moretti[2], Kassa Belay Ibrahim[2,*], and Najoua Turki-Kamoun[1]

[1] *Laboratory of Condensed Matter Physics, Faculty of Sciences of Tunis, University of Tunis El Manar, 2092 Tunis, Tunisia*
[2] *Department of Molecular Sciences and Nanosystems, Ca' Foscari University of Venice, Via Torino 155, 30172 Venice, Mestre, Italy*
[3] *Division of Materials Science, Department of Engineering Sciences and Mathematics, Luleå University of Technology, 97187 Luleå, Sweden*

Received: 11 August 2025
Accepted: 20 October 2025
Published online: 6 November 2025

ABSTRACT

The removal of pharmaceutical pollutants from water remains a critical environmental challenge, necessitating photocatalytic materials with efficient charge separation and high conductivity. Here, we report the first synthesis of graphene (Gra)–$ZnFe_2O_4$ nanocomposite thin films via spray pyrolysis, successfully overcoming the major limitations of pristine zinc ferrite, namely, its wide band gap, low electrical conductivity, and rapid electron–hole recombination through Gra incorporation. The resulting nanocomposite demonstrates promising performance in the photocatalytic degradation of ampicillin, highlighting its potential for pharmaceutical pollutant remediation. The effect of Gra integration was thoroughly confirmed through structural, morphological, optical, and electrical characterization, which revealed strong interfacial contact between Gra and $ZnFe_2O_4$ nanoparticles. Gra acts as an electron acceptor and conductive network, enhancing charge separation, suppressing electron–hole recombination, and facilitating electron mobility. Consequently, the optical band gap decreased from 3.01 to 2.77 eV, and electrical resistivity dropped from 187.1 to 177.2 Ω. The optimized nanocomposite achieved 60% degradation of ampicillin under visible light, demonstrating significantly enhanced photocatalytic performance. These results establish Gra–$ZnFe_2O_4$ thin films as a scalable, efficient, and sustainable platform for water treatment, combining tunable optical properties, high surface area, and superior charge carrier dynamics.

Handling Editor: Ivo Teixeira.

Address correspondence to E-mail: dhiffatmaezzahra@gmail.com; kassabelay.ibrahim@unive.it

https://doi.org/10.1007/s10853-025-11719-3

Introduction

Pharmaceutical pollution, particularly contamination by antibiotics, has emerged as a critical environmental challenge in recent decades [1]. Among these pollutants, the ampicillin antibiotic, widely used in human and veterinary medicine, has been frequently detected in surface water and wastewater effluents [2]. Its strong chemical stability, resistance to biodegradation, and potential to induce antimicrobial resistance make it a high-priority contaminant for removal [3]. Conventional water treatment processes, including biological filtration and chlorination, are largely ineffective at degrading such persistent pharmaceutical compounds [4]. This growing threat has accelerated the development of advanced oxidation processes (AOPs), with photocatalytic degradation gaining particular attention due to its high efficiency, environmental compatibility, and ability to completely mineralize pollutants under light irradiation [5]. Photocatalysis employs semiconductors that, upon exposure to light, generate reactive species capable of degrading organic pollutants. Among visible light responsive photocatalysts, zinc ferrite ($ZnFe_2O_4$) has attracted considerable interest due to its narrow band gap, chemical stability, photochemical robustness, and magnetic properties. Its spinel structure and ability to absorb in the visible spectrum make it a viable candidate for photocatalytic water treatment [6, 7]. However, the low electrical conductivity and high electron–hole recombination rate of pristine $ZnFe_2O_4$ limit its photocatalytic efficiency, particularly under visible light.

To address these limitations, considerable research has focused on the development of $ZnFe_2O_4$-based nanocomposites incorporating conductive materials. Graphene (Gra), a two-dimensional carbon nanomaterial, is particularly promising due to its extraordinary electrical conductivity, high surface area, mechanical strength, and electron mobility [8]. When coupled with metal oxides such as $ZnFe_2O_4$, Gra serves as a conductive network that enhances charge separation, facilitates electron transport, and suppresses recombination, thereby boosting photocatalytic activity. Several studies have demonstrated that Gra-integrated ferrite nanocomposites show significant improvements in electrical, magnetic, and catalytic performance. For example, Abbas et al. (2024) synthesized Gra–Co–Zn ferrites via sol–gel auto-combustion, reporting enhanced thermoelectric behaviour [9], while Ullah Khan et al. (2024) found that integrating Gra nanoplatelets improved the electronic properties of Ni–Zn–Cd ferrites [10]. While most Gra–ferrite composites have been studied in powder form, thin films offer additional advantages for practical applications. Nanocomposite thin films provide better control over morphology, interface behaviour, and film thickness parameters critical for optimizing light absorption, charge transport, and surface reactions in photocatalytic processes [11]. Moreover, thin films can be directly integrated into microelectronic and optoelectronic devices, enabling scalable and reproducible fabrication.

Among thin film deposition techniques, spray pyrolysis was selected for its simplicity, cost-effectiveness, scalability, and ability to produce uniform coatings on various substrates [12]. It allows precise tuning of film composition and thickness, making it ideal for fabricating nanocomposite thin films for environmental and energy-related applications. Despite the growing interest in Gra–$ZnFe_2O_4$ composites, no studies to date have reported their fabrication as thin films via spray pyrolysis for the photocatalytic degradation of ampicillin. This represents a significant research gap, especially considering the environmental urgency to develop efficient methods for removing persistent antibiotics from water.

In this study, we report, for the first time, the synthesis of Gra–$ZnFe_2O_4$ nanocomposite thin films using the spray pyrolysis technique and investigate their photocatalytic activity towards the degradation of ampicillin under visible light irradiation. Thin films with varying Gra content ($x = 0$, 2, 4, and 8 wt%) were deposited on glass substrates. The resulting films were systematically characterized in terms of their structural, morphological, optical, and electrical properties. The photocatalytic performance of these nanocomposites was evaluated with a focus on the influence of Gra incorporation on ampicillin degradation and recorded 60% efficiency. This work not only contributes to the design of advanced photocatalytic materials but also addresses a critical environmental challenge through the development of a novel thin film-based degradation platform.

Experimental section

Synthesis of Gra–$ZnFe_2O_4$ nanocomposite thin films

Gra–$ZnFe_2O_4$ nanocomposite thin films were synthesized via aerosol-assisted spray pyrolysis on

pre-cleaned glass substrates (Fig. 1a). Substrate preparation involved sequential ultrasonication in acetone (10 min) and ethanol (10 min), followed by thorough rinsing with deionized water (18.2 MΩ·cm) and dried in a muffle furnace to ensure optimal surface purity. The precursor solution was formulated by dissolving zinc acetate dihydrate ($Zn(CH_3COO)_2{\cdot}2H_2O$, 99.99%) and iron(III) chloride hexahydrate ($FeCl_3{\cdot}6H_2O$, 98%) in a 1:2 molar ratio ($Zn^{2+}/Fe^{3+} = 0.5$) within a propanol/water (3:1 v/v) solvent mixture, acidified with glacial acetic acid (0.1 vol%) to enhance sol stability. For the Gra–$ZnFe_2O_4$ nanocomposite, a graphene oxide (GO) aqueous dispersion (Graphene, 4 mg/mL, monolayer content > 95%) was diluted to obtain a final concentration of 1.65×10^{-3} M before incorporation into the precursor solution. During the subsequent spray pyrolysis (450 °C) and annealing (500 °C), the GO underwent thermal reduction to graphene nanosheets, yielding the final Gr–$ZnFe_2O_4$ nanocomposite thin films. The Zn/Gra weight ratio was adjusted from 0 to 8% to modulate composite properties. The deposition was carried out at a substrate temperature of 450 ± 5 °C, maintained using a PID-controlled hotplate. The nozzle-to-substrate distance was fixed at 27 cm to ensure uniform film morphology, while the spray rate was kept constant at 10 mL/min using compressed air as the carrier gas. Post-deposition, all samples were annealed at 500 °C for 2 h in static air (5 °C/min ramp rate) to enhance crystallinity and reduce lattice strain.

Structural and functional characterization

The crystalline structure of the films was analysed by X-ray diffraction (XRD, Bruker D8 Advance, Cu Kα radiation, $\lambda = 1.5418$ Å) to determine phase purity and crystallite size. Surface morphology and elemental composition were examined using scanning electron

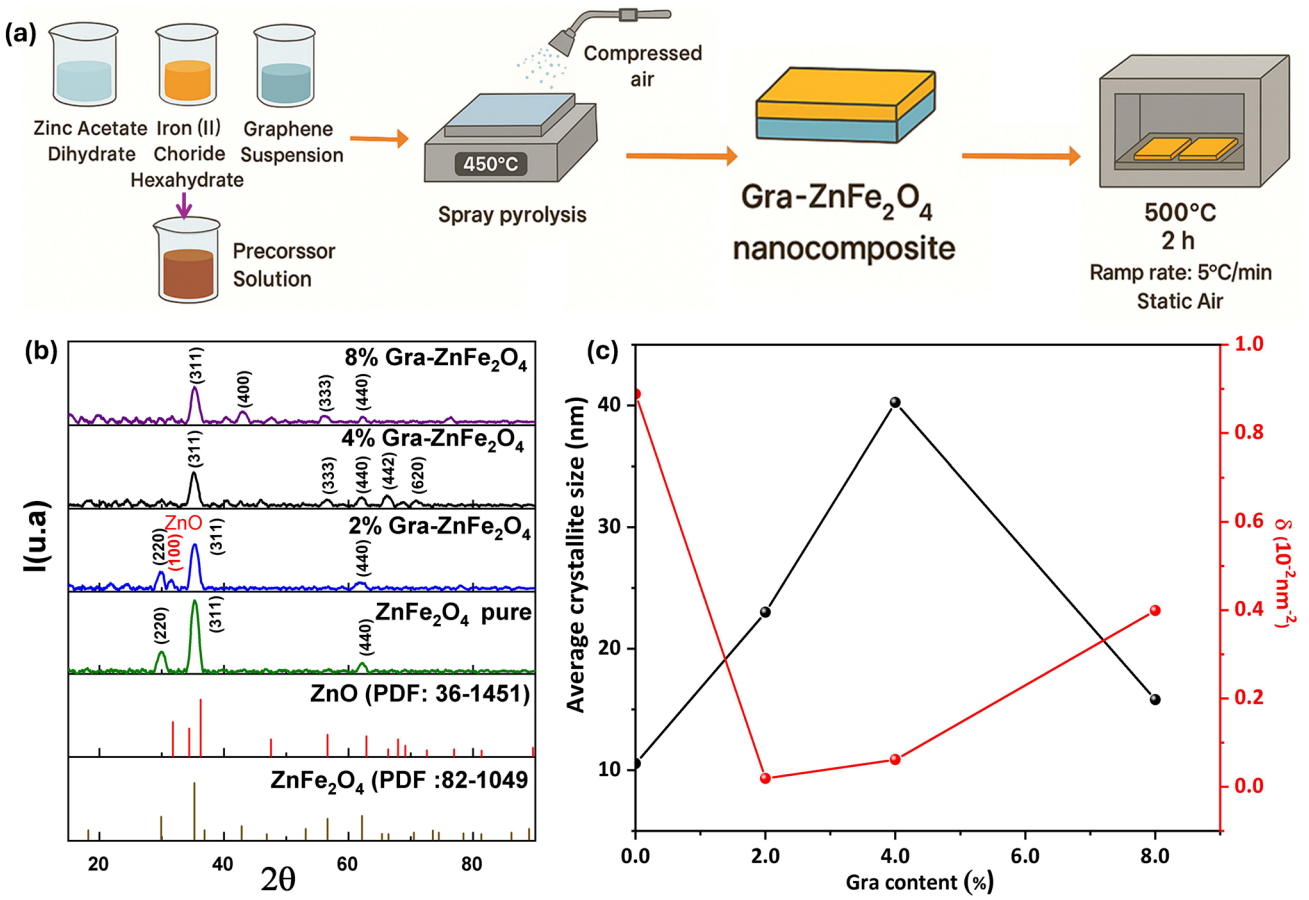

Figure 1 **a** Schematic representation for the synthesis process of Gra–$ZnFe_2O_4$ thin films by spray pyrolysis. **b** XRD patterns of the pristine and Gra–$ZnFe_2O_4$ nanocomposite thin films at different Gra concentrations. **c** The variation of both average crystallite size (D) and dislocation density (δ) with 0, 2, 4, and 8% graphene contents.

microscopy (SEM) coupled with energy-dispersive X-ray spectroscopy (EDX). Atomic force microscopy (AFM, Bruker Dimension Icon, tapping mode) provided high-resolution topographical data, including root-mean-square (RMS) roughness. Optical properties were investigated via UV–Vis–NIR spectroscopy (PerkinElmer LAMBDA 950) equipped with an integrating sphere, allowing for accurate reflectance and transmittance measurements across 250–1500 nm. Band gap energies were derived from Tauc plots, while photoluminescence (PL) spectroscopy (PerkinElmer LS55, excitation at 300 nm) probed defect-related emission and charge recombination dynamics. Electrical characterization was performed using impedance spectroscopy (Agilent E4980A, 20 Hz–2 MHz) to evaluate conductivity under varying frequencies.

Photocatalytic degradation of ampicillin

The photocatalytic activity of the Gra–$ZnFe_2O_4$ nanocomposites was evaluated through the degradation of ampicillin (10 mg/L) under natural sunlight exposure to simulate real-world environmental remediation conditions. Before irradiation, the films were immersed in 50 mL of antibiotic solution and maintained in darkness for 30 min to establish adsorption–desorption equilibrium, ensuring subsequent measurements solely reflected photocatalytic processes. Following dark equilibration, the samples were exposed to natural sunlight to initiate photocatalytic degradation. Sunlight experiments were conducted during peak solar intensity hours (10:00–14:00) under clear sky conditions. The experimental setup allowed for a systematic comparison between adsorption under dark conditions and photodegradation under solar irradiation, providing critical insights into the nanocomposite's potential for wastewater remediation.

Results and discussion

Morphological and structural characterization

To confirm the crystallographic structure for pristine ferrite and Gra–zinc ferrite nanocomposite, XRD was employed. As shown in Fig. 1b, XRD patterns of pristine $ZnFe_2O_4$ and Gra-incorporated $ZnFe_2O_4$ nanocomposite thin films with varying Gra loadings (0, 2, 4, and 8 wt%). The XRD results confirm the polycrystalline nature of all samples, as evidenced by multiple diffraction peaks corresponding to distinct crystallographic planes. Prominent reflections peaks appeared at 2θ values of 29.9°, 35.3°, 36.9°, 42.8°, 56.6° 62.2, 66.4°, and 70.6°, which correspond to the (220), (311), (222), (400), (333), (422) (440), (442), and (620) planes of $ZnFe_2O_4$, respectively. This matches well with the standard diffraction data (JCPDS PDF#22–1049), confirming the formation of a cubic spinel structure. Among the diffraction patterns, the (311) reflection appears as the most intense peak, indicating a preferred crystallographic orientation of $ZnFe_2O_4$ along this plane. With increasing graphene content, however, the intensity of the (311) peak gradually decreases, reflecting a reduction in crystallinity due to lattice strain and structural disorder induced by graphene incorporation, which disrupts the long-range order of the spinel lattice [13]. Moreover, additional reflections are observed after Gra incorporation. The appearance of these peaks indicates a change in the orientation of the crystallites after doping. This evolution in diffraction patterns implies that graphene incorporation significantly influences the crystallographic texture of the nanocomposite films, potentially promoting preferential growth or realignment of crystallites along specific orientations [14].

We note also that the XRD pattern of the 2 wt% Gra–$ZnFe_2O_4$ sample exhibits an additional diffraction peak at $2\theta \approx 31.6°$, which corresponds to the (100) plane of ZnO (JCPDS card no. 36–1451). This observation suggests a partial reduction or decomposition of $ZnFe_2O_4$ during the synthesis process induced by the reductive nature of Gra. It is worth mentioning that no distinct diffraction peak of graphene (typically expected near $2\theta \approx 26°$ for the (002) reflection) is observed in any of the composites. The absence of graphene peaks can be attributed to its relatively low content within the $ZnFe_2O_4$ matrix. Similar observations have been reported in other graphene oxide composites, where graphene peaks were not detected due to their low content and weak diffraction signals [15, 16]. The variation of average crystallite size (D) and dislocation density (δ) of $ZnFe_2O_4$ with different Gra contents, as depicted in Fig. 1c and in Table 1, reveals a clear structural evolution influenced by the incorporation of Gra. XRD results reveal significant changes in average crystallite size and dislocation density (δ) with increasing graphene content in $ZnFe_2O_4$ nanocomposites. The pristine $ZnFe_2O_4$ shows the smallest crystallite size (10.6 nm) but the highest dislocation density (0.889×10^{-2} nm^{-2}), indicating a highly

Table 1 Grain size (D) and dislocation density (δ) values of pristine $ZnFe_2O_4$ and Gra–$ZnFe_2O_4$ nanocomposites

Samples	Pristine $ZnFe_2O_4$	2% Gra–$ZnFe_2O_4$	4% Gra–$ZnFe_2O_4$	8% Gra–$ZnFe_2O_4$
Average crystallite size (nm)	10.6 ± 0.14	23.0 ± 1.22	40.3 ± 3.16	15.8 ± 0.56
δ.10–2(nm-2)	0.889	0.0189	0.0616	0.0399

defective structure that can hinder photocatalytic performance by promoting charge carrier recombination. Adding graphene at 2% and 4% increases crystallite size to 23 nm and 40.3 nm, while reducing δ, suggesting improved crystallinity but at the cost of reduced surface area. In contrast, the 8% Gra–$ZnFe_2O_4$ sample achieves an ideal compromise with a moderate crystallite size (15.8 nm) and a relatively low dislocation density (3.99×10^{-4} nm^{-2}). This structure offers enhanced surface area for photocatalytic reactions, while maintaining good crystallinity to support efficient charge separation. Therefore, based on the balance between nanoscale particle size and structural quality, 8% Gra–$ZnFe_2O_4$ is expected to deliver the best performance in photodegradation applications.

The surface morphology and microstructural features of pristine $ZnFe_2O_4$ and 8% Gra–$ZnFe_2O_4$ nanocomposite were examined using SEM at various magnifications, as depicted in Fig. 2 (a–f). Figure 2(a-c) presents the SEM images of pristine $ZnFe_2O_4$ at scales of 2 µm, 1 µm, and 200 nm, respectively. The pristine $ZnFe_2O_4$ samples exhibit densely packed and agglomerated particles with irregular morphology. At higher magnification (Fig. 2c), $ZnFe_2O_4$ nanoparticles appear quasi-spherical or faceted, yet closely bound, indicating minimal dispersion and restricted

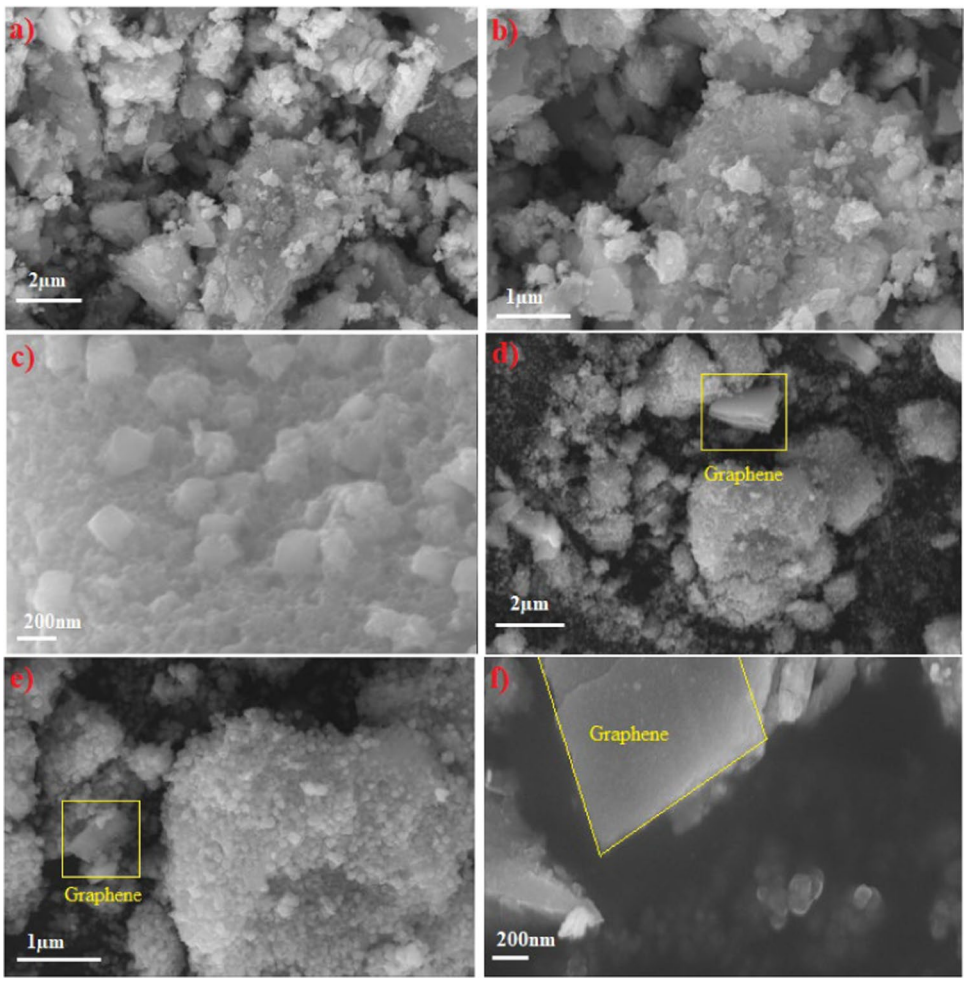

Figure 2 SEM images at different magnifications, 2 µm, 1 µm, and 200 nm of **a–c** pristine $ZnFe_2O_4$; and **d–e** 8% Gra–$ZnFe_2O_4$ nanocomposite.

active surface area. In contrast, the SEM images of the 8% Gra–$ZnFe_2O_4$ nanocomposite (Fig. 2d-f) reveal a markedly different morphology. The presence of Gra is clearly observed as thin, flake-like sheets (highlighted in yellow), serving as a supportive scaffold for $ZnFe_2O_4$ nanoparticle deposition. At lower magnification (Fig. 2d), Gra sheets are embedded within the composite structure, leading to a more open and porous morphology. As shown in Fig. 2d, $ZnFe_2O_4$ nanoparticles are uniformly distributed and well-anchored on the Gra surface, effectively reducing agglomeration. At the nanoscale (Fig. 2f), the Gra sheet provides a high surface area platform for $ZnFe_2O_4$ nanoparticle attachment, promoting strong interfacial contact. This synergistic integration of Gra enhances particle dispersion, electrical conductivity, and surface accessibility, critical factors for applications such as photocatalysis and energy storage. Overall, the SEM analysis confirms that Gra incorporation significantly modifies the morphology of $ZnFe_2O_4$, facilitating the formation of a well-dispersed nanocomposite architecture due to the high surface area of Gra.

EDX spectroscopy was also employed to confirm the presence of elements in the respective samples. As shown in Fig. 3a, the spectrum of pristine $ZnFe_2O_4$ displays characteristic peaks corresponding to Zn, Fe, and O, confirming the presence of the expected elements in the spinel ferrite structure. In the case of the 8% Gra–$ZnFe_2O_4$ nanocomposite (Fig. 3b), in addition to the peaks of Zn, Fe, and O, a distinct peak corresponding to C is observed from Gra, clearly indicating the successful incorporation of Gra into the nanocomposite. The detected Cl peak may be attributed to residual chloride from the iron precursor.

Fourier transform infrared (FTIR) spectroscopy

Figure 3c presents the FTIR spectra of pristine $ZnFe_2O_4$ and 8% Gra–$ZnFe_2O_4$ nanocomposite, confirming their successful synthesis through the identification of characteristic functional groups. In the pristine $ZnFe_2O_4$ spectrum, absorption bands observed at 3430.5 cm^{-1} and 1381 cm^{-1} correspond to O–H stretching vibrations of adsorbed water molecules and metal–oxygen

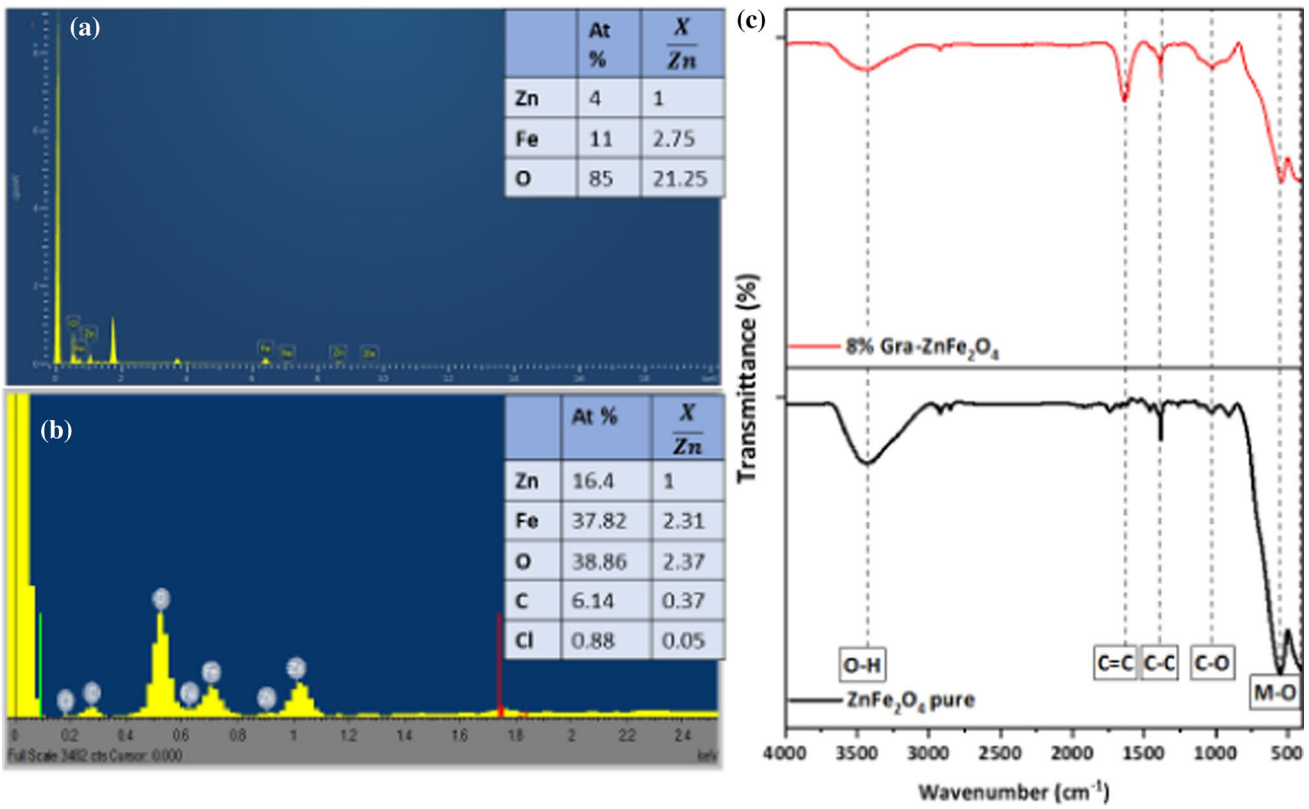

Figure 3 EDX spectrum of **a** $ZnFe_2O_4$, **b** 8% Gra–$ZnFe_2O_4$ nanocomposite, and **c** FTIR spectra of pristine and 8% Gra–$ZnFe_2O_4$ nanocomposite.

interactions, respectively [17]. A strong absorption band observed at 558.9 cm^{-1} corresponds to the Fe–O stretching vibrations in the tetrahedral sites, while the band around 417.5 cm^{-1} is attributed to the bending vibrations of metal–oxygen bonds in the octahedral sites. [18–21]. For the 8% Gra–$ZnFe_2O_4$ nanocomposite, the spectrum exhibits a broad peak at 3462.5 cm^{-1}, which indicates enhanced O–H stretching due to increased surface hydroxyl groups and possible hydrogen bonding with graphene. The appearance of peaks at 1631.52 and 1025.02 cm^{-1} can be assigned to C=C skeletal vibrations and C–O stretching from the graphene component, confirming successful incorporation of graphene into the ferrite matrix [22]. Additionally, the characteristic metal–oxygen bands at 548.21 and 417.59 cm^{-1} remain evident, demonstrating that the spinel structure of $ZnFe_2O_4$ is preserved after graphene integration.

Atomic force microscopy (AFM)

To further investigate the effect of Gra incorporation on the surface roughness and grain structure of $ZnFe_2O_4$ thin films, Atomic Force Microscopy (AFM) was employed. The AFM images presented in Fig. 4 offer detailed insight into the surface morphology before and after the addition of Gra. The pristine $ZnFe_2O_4$ thin film (Fig. 4d) exhibits a relatively smooth and uniform surface with well-defined grains averaging around 40 nm in size and a root-mean-square (RMS) roughness of 2.19 nm. Upon incorporation of 8 wt% Gra (Fig. 4e), the surface becomes noticeably rougher, with smaller grain sizes averaging approximately 30 nm and an increased RMS roughness of 2.55 nm, indicating enhanced surface texture and possible modification of the nucleation and growth behaviour due to Gra. The reduction in grain size upon Gra incorporation increases the density of grain boundaries, which are often associated with enhanced photocatalytic activity due to the availability of more reactive sites and improved charge separation. This reduction in grain size suggests that Gra acts as a growth inhibitor, disrupting agglomeration and promoting finer crystallite formation during film deposition. The increased surface roughness, on the other hand, enhances the effective surface area, potentially providing more active sites for photocatalytic reactions.

Such microstructural changes are highly advantageous for the photocatalytic degradation of pollutants such as ampicillin. The smaller grain size increases grain boundary density, which can serve as active sites for charge separation and pollutant interaction. The enhanced roughness facilitates greater light scattering and adsorption of pollutant molecules, while the presence of Gra is expected to improve charge carrier transport and reduce electron–hole recombination. Similar trends have also been observed in the photocatalytic degradation of Congo Red dye, where a reduction in particle size was shown to increase surface area and improve degradation efficiency through enhanced [23].

Optical characterization

The UV–Vis–NIR optical properties of $ZnFe_2O_4$ and Gra–$ZnFe_2O_4$ nanocomposites with varying content of Gra were investigated to determine their reflectance and energy band gap. The reflectance spectra of all the samples are presented in Fig. 5a. The pristine $ZnFe_2O_4$ thin films demonstrated the highest reflectance in the visible region, indicating its lower light absorption. The incorporation of Gra into $ZnFe_2O_4$ is associated with a decrease in reflectance. This reduction can be explained by the inclusion of additional energy levels within the band gap due to the Gra incorporation, which facilitates electronic transitions and enhances light absorption.

Energy band gap values have been determined from Tauc plots and are shown in Fig. 5b. The specific values of Eg for the pristine and Gra–$ZnFe_2O_4$ nanocomposite are summarized in Table 2. It is found that E_g decreased from 3.01 eV for the pristine $ZnFe_2O_4$ nanofilms to 2.77 eV for 8% Gra–$ZnFe_2O_4$ nanocomposites. The incorporation of Gra into zinc ferrite nanocomposites has significantly influenced its optical band gap. A variety of studies in the literature present a reduction in Eg values of title composites due to the addition of Gra, corresponding to the possibility of interaction between the 3d orbitals of Fe^{3+} ions and the 2p electron states of oxygen [24, 25]. It is noted that bulk $ZnFe_2O_4$ has a reported band gap of ~ 1.9 eV [26], while nanostructured $ZnFe_2O_4$ can exhibit higher values, as observed here (3.01 eV). The optical band gap is highly sensitive to synthesis conditions, particle size, cation distribution, and chemical environment. Similar variations have been reported by Ikramullah et al. for $ZnFe_2O_4$ nanoparticles, with band gaps of 2.49–2.77 eV depending on pH [27], and by Doiphode et al. for nanostructured

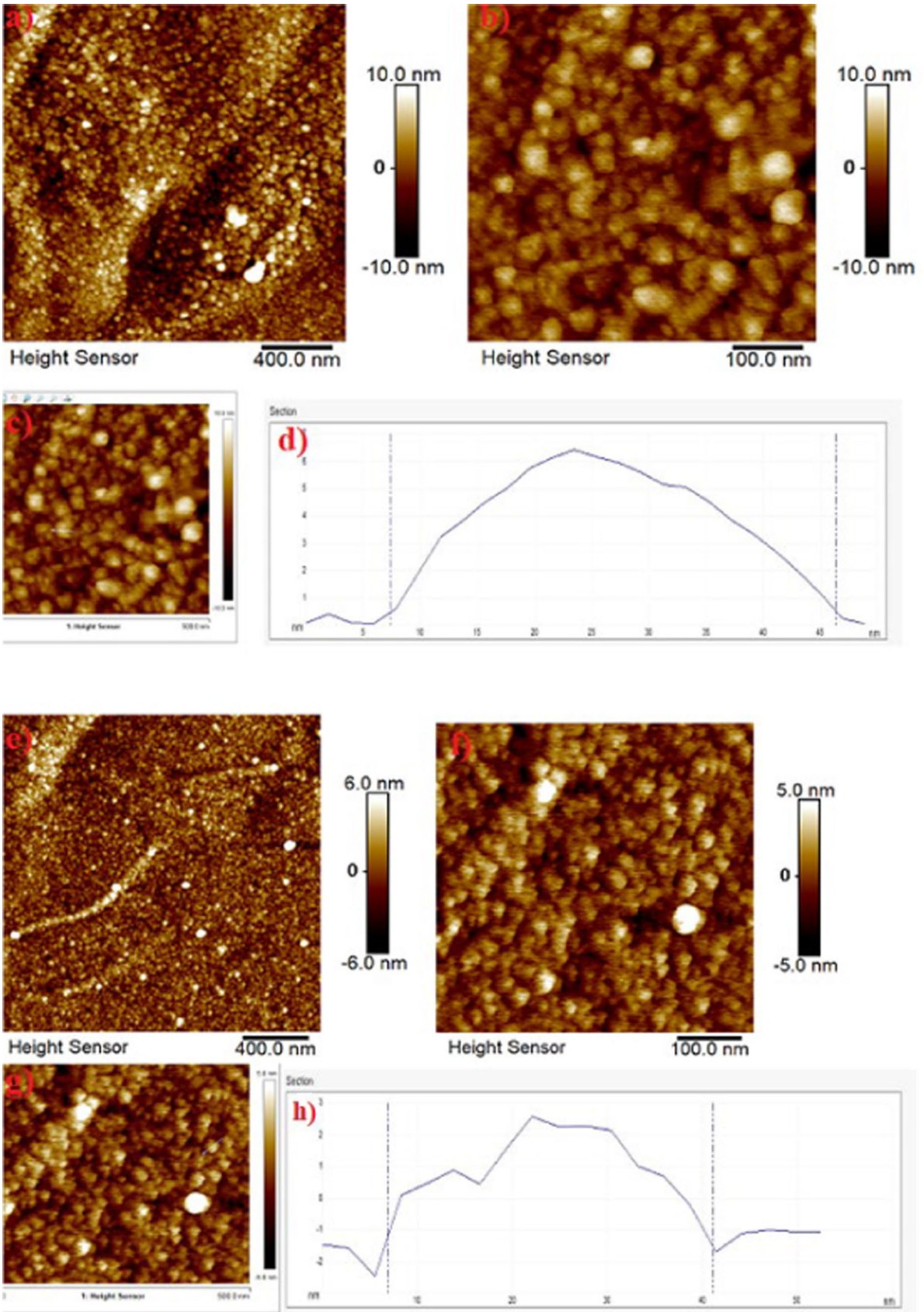
a)
10.0 nm
0
-10.0 nm
Height Sensor
400.0 nm
b)
10.0 nm
0
-10.0 nm
Height Sensor
100.0 nm
c)
d)
Section
e)
6.0 nm
0
-6.0 nm
Height Sensor
400.0 nm
f)
5.0 nm
0
-5.0 nm
Height Sensor
100.0 nm
g)
h)
Section

◂**Figure 4** AFM images and grain size at 400 nm, 100 nm, and 500 nm for **a–d** pristine $ZnFe_2O_4$ and **e–h** 8% Gra–$ZnFe_2O_4$, respectively.

$ZnFe_2O_4$ thin films, with band gaps of 2.21–3.21 eV depending on Fe concentration and processing conditions [28]. These factors collectively influence the electronic structure and optical behaviour of $ZnFe_2O_4$.

Photoluminescence (PL) analysis

PL emission is due principally to the direct recombination of the excited electrons and holes. To investigate the charge separation process and the fate of the photogenerated electron–hole pair, the PL emission analysis was performed. Room temperature PL spectra of pristine $ZnFe_2O_4$ and x Gra–$ZnFe_2O_4$ ($x = 2$, 4, and 8%) nanocomposites are illustrated in Fig. 6. In the visible region, two emission peaks at around 424 nm and 502 nm were identified for both pristine $ZnFe_2O_4$ and Gra–$ZnFe_2O_4$ nanocomposites with different Gra contents at an excitation wavelength of 300 nm. A similar result was found by Renuka et al. [29]. It can be observed that the emission of pristine $ZnFe_2O_4$ is centred at 424 nm, which is attributed to the recombination of holes and electrons in the valence and conduction bands. The incorporation of Gra in the zinc ferrite thin films induces a shift of this peak to a higher wavelength (lower energy), which is in good agreement with the band gap energy analysis.

Interestingly, there was no discernible shift in the positions of the PL peak at 502 nm between the pristine and Gra–$ZnFe_2O_4$ nanocomposite samples. The green emission peak observed around 502 nm indicates the presence of singly ionized oxygen vacancies, arising from the recombination of a photogenerated hole with the singly ionized charge state of this defect [30]. Moreover, as presented in the PL spectra, the increase of Gra content is followed by a decrease of PL intensity. Photoluminescence spectra with high-emission intensity are associated with a high recombination rate of photogenerated charge carriers and conversely [31]. The intensity reached a maximum value for pristine $ZnFe_2O_4$. However, because of the inclusion of Gra, the PL intensity decreases significantly, demonstrating a high electron–hole separation efficiency (low recombination rate).

Electrochemical impedance spectroscopy analysis (EIS):

The electrochemical impedance spectroscopy analysis is used to determine the effect of Gra on the electrical properties of zinc ferrite thin films. We note that the radius of the semicircle is directly related to the charge transfer resistance (Rct). Figure 7 illustrates EIS results for the pristine $ZnFe_2O_4$ and 8% Gra–$ZnFe_2O_4$ nanocomposite under visible light. The data from these plots were simulated and fitted using an equivalent electrical circuit depicted in the same figure.

The Nyquist plot shows that the radius of the semicircle decreases, indicating a reduction in charge transfer resistance from 54.23 kΩ for the pristine $ZnFe_2O_4$ to 45.35 kΩ for the 8% Gra–$ZnFe_2O_4$ nanocomposite, as shown in Table 3. This means that the conductivity of the films has improved. As a result, the 8% Gra–$ZnFe_2O_4$ nanocomposites exhibit significantly enhanced electrical performance compared to the pristine $ZnFe_2O_4$ nanofilms, indicating an improvement in overall charge transport and conductivity (Table 4).

Application of graphene–$ZnFe_2O_4$ thin films for ampicillin degradation

Photodegradation of ampicillin under visible light

The widespread use of ampicillin (AMP) in medical and veterinary applications has led to its persistent accumulation in aquatic environments, raising significant concerns due to its potential toxicity, role in antibiotic resistance, and ecological risks [32]. To mitigate these threats, extensive research efforts have focused on developing advanced photocatalytic materials capable of degrading such pharmaceutical pollutants. Among these, metal oxides, particularly spinel ferrites like zinc ferrite ($ZnFe_2O_4$), have garnered considerable attention due to their high chemical stability, visible light responsive band gap, and magnetic recoverability. However, to further enhance their photocatalytic efficiency, recent studies have explored the incorporation of Gra as a novel strategy to improve charge separation and light absorption. Gra's exceptional electron mobility acts as an electron sink, reducing recombination losses, while its large surface area enhances pollutant adsorption and active site availability. Notably, this study presents the first

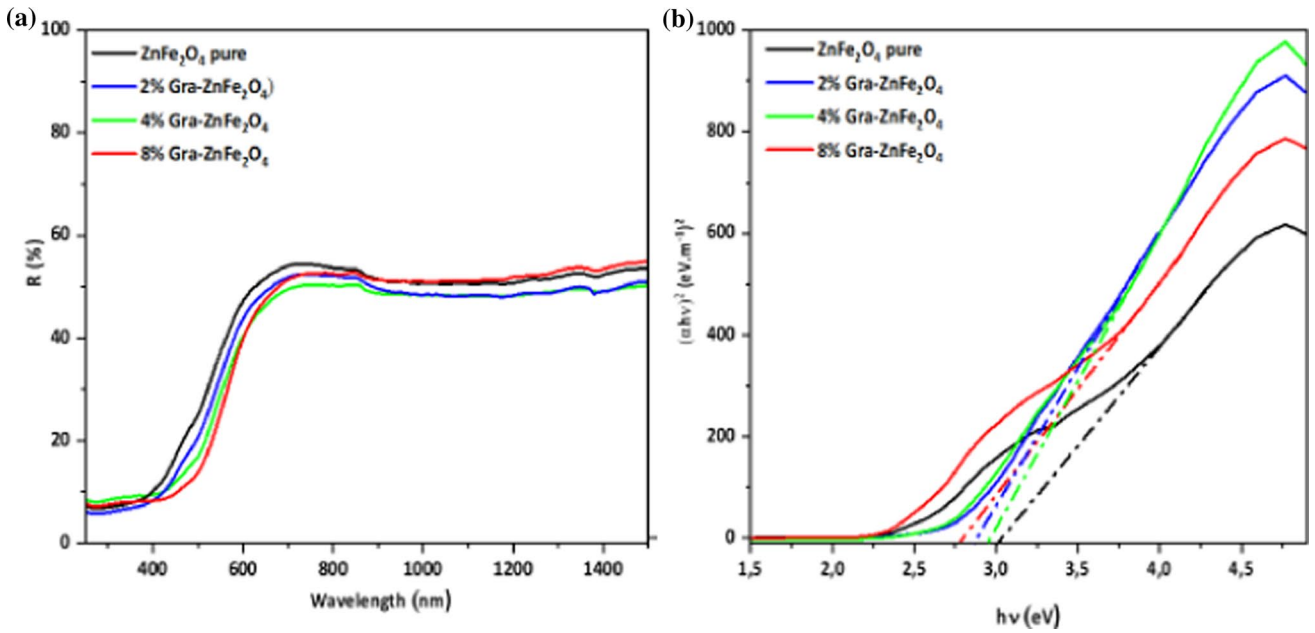

Figure 5 **a** Reflection spectra and **b** Tauc plot generated for pristine $ZnFe_2O_4$ and (2, 4, and 8%) Gra–$ZnFe_2O_4$ nanocomposite thin films.

Table 2 Band gap energy of pristine $ZnFe_2O_4$ and Gra–$ZnFe_2O_4$ nanocomposites

Samples	Eg (eV)
Pristine $ZnFe_2O_4$	3.01
2% Gra–$ZnFe_2O_4$	2.86
4% Gra–$ZnFe_2O_4$	2.96
8% Gra–$ZnFe_2O_4$	2.77

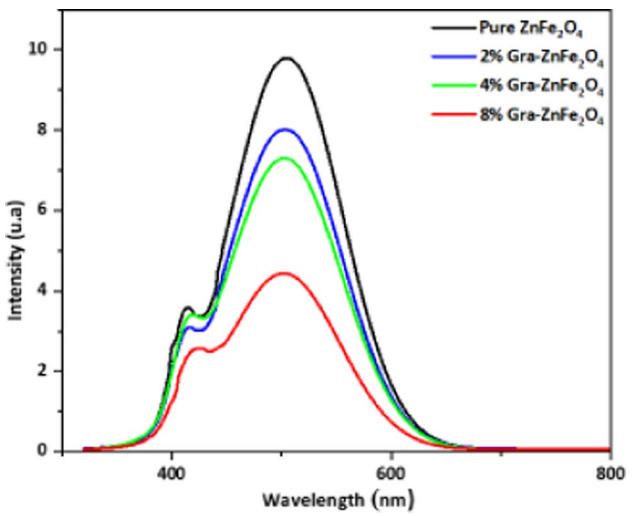

Figure 6 Photoluminescence (PL) emission spectra of pristine $ZnFe_2O_4$ and graphene–$ZnFe_2O_4$ nanocomposites with different graphene loadings ($x = 2$, 4, and 8 wt%). Measurements were performed at room temperature with an excitation wavelength of 300 nm.

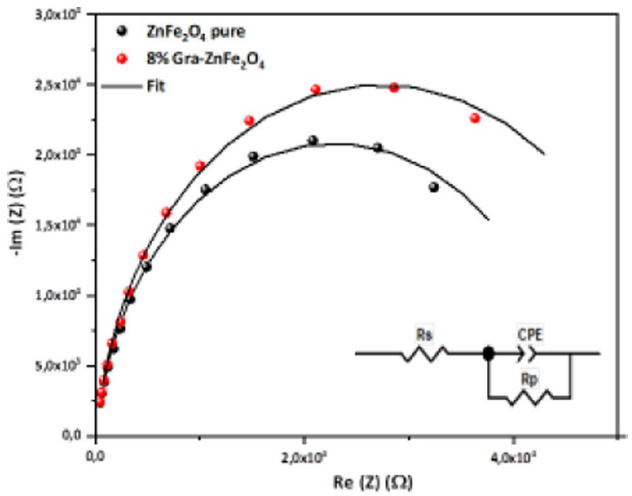

Figure 7 Nyquist plots of pristine $ZnFe_2O_4$ and 8 wt% graphene–$ZnFe_2O_4$ nanocomposite measured by electrochemical impedance spectroscopy (EIS) at room temperature over the frequency range of 20 Hz–2 MHz and a fixed potential of 1 V. The inset shows the equivalent circuit model used to extract electrical parameters, including series resistance (R_s), parallel resistance (R_p), and a constant phase element (CPE), which reflect the charge transfer and conductivity properties of the samples.

investigation of Gra–$ZnFe_2O_4$ nanocomposite thin films for the photocatalytic degradation of ampicillin, offering new insights into the synergistic effects

Table 3 The fitting values of the impedance spectra of pristine $ZnFe_2O_4$ and 8% Gra–$ZnFe_2O_4$ nanocomposite

Electrical parameters	Rs (Ω)	Rp (kΩ)	CPE-T (F)	CPE-P (F)
Pristine $ZnFe_2O_4$	187.1	54.23	9.089E-11	0.94866
8% Gra–$ZnFe_2O_4$	175.2	45.35	9.778E-11	0.94595

between Gra and spinel ferrites for environmental remediation applications.

The absorption spectra of ampicillin (Fig. 8a) exhibited a rapid decline in peak intensity, indicating significant degradation over time. The enhancement in photocatalytic activity is clearly reflected in the experimental results, as shown in the degradation kinetics (Fig. 8b). The photocatalytic efficiency was determined using the equation:

$$\text{Efficiency}(\%) = \frac{C_0 - C}{C_0} \times 100$$

where C_0 and C represent the initial and final concentrations of ampicillin, respectively.

Among the tested compositions, the 8 wt% graphene–$ZnFe_2O_4$ (Gra–$ZnFe_2O_4$) nanocomposite demonstrated the highest efficiency, achieving 60% degradation after 2 h of sunlight irradiation (Fig. 8c). This superior performance can be attributed to the incorporation of graphene, which enhances light absorption, improves charge carrier separation, and reduces electron–hole recombination. Similar studies have been reported in related graphene–metal oxide systems, such as ZnO/GO [33], N-doped graphene/TiO_2 [34], and VOx–GO composites, where small amounts of graphene significantly improve photocatalytic activity, but higher loadings lead to aggregation, light shielding, or reduced exposure of active sites [35]. Based on these literature precedents and our observations, 8 wt% graphene was chosen as the upper limit in this study, as further increases are likely to result in diminishing returns or reduced efficiency.

The conductive Gra network facilitates faster electron transfer, while the $ZnFe_2O_4$ matrix provides active sites for radical generation (e.g., •OH and $•O_2^-$), leading to more efficient ampicillin breakdown. This photocatalytic efficiency is particularly noteworthy when evaluated against the existing literature. The degradation of β-lactam antibiotics like ampicillin is widely recognized as a complex and challenging process due to the molecule's high structural stability and resistance to photolytic breakdown. For example, Nosrati et al. reported only 41% degradation of ampicillin after 120 min using a ZnO/polyaniline nanocomposite under similar sunlight conditions [36]. In contrast, our system demonstrates superior activity using a thin film photocatalyst under real sunlight exposure. Comparative studies on other antibiotics show degradation efficiencies ranging from 48 to 65%, but often under more favourable conditions such as UV light irradiation, higher catalyst dosages, or extended reaction times. For instance, ciprofloxacin reached 60% degradation after 300 min using 5.0 g/L CuO under visible light [41], and sulphamethazine degradation using Bi_2WO_6/RGO took up to 8 h under simulated sunlight to achieve similar outcomes [44]. Compared to these,

Table 4 Comparison of photocatalytic degradation efficiencies for antibiotic removal in recent studies

No	Antibiotic	Photocatalyst	Light source	Initial conc. (mg/L)	Catalyst dose (g/L)	Degradation (%)	Time (min)	Ref
1	Ampicillin	ZnO/polyaniline	Sunlight	4.5	0.01	41.0%	120	[36]
2	Metronidazole	ZnO–$ZnAl_2O_4$	Sunlight	20.0	0.4	50.0%	120	[37]
3	Amoxicillin	TiO_2	UV light	10.0	0.25	65.0%	150	[38]
4	Amoxicillin	Iron nanoparticle (IPP)	Visible light	10.0	2.5	60.0%	60	[39]
5	Norfloxacin	Ni_2O_3@PC	UV light	10.0	0.1	59.0%	180	[40]
6	Ciprofloxacin	CuO	Visible light	10.0	5.0	60.0%	300	[41]
7	Sulphanilamide	Mo–BiOBr	Visible light	10.0	0.3	48.3%	80	[42]
8	Sulphamethazine	Graphene aerogel/Bi_2WO_6	Simulated sunlight	10.0	—	55.8%	120	[43]
9	Sulphamethazine	Bi_2WO_6/RGO	Simulated sunlight	10.0	—	57.6%	480	[44]
10	Sulphamethazine	TiO_2	UV light	20.0	0.5	61.0%	120	[45]
11	Ampicillin	Gra–$ZnFe_2O_4$ thin film	Natural sunlight	10.0	-	60.0%	120	This work

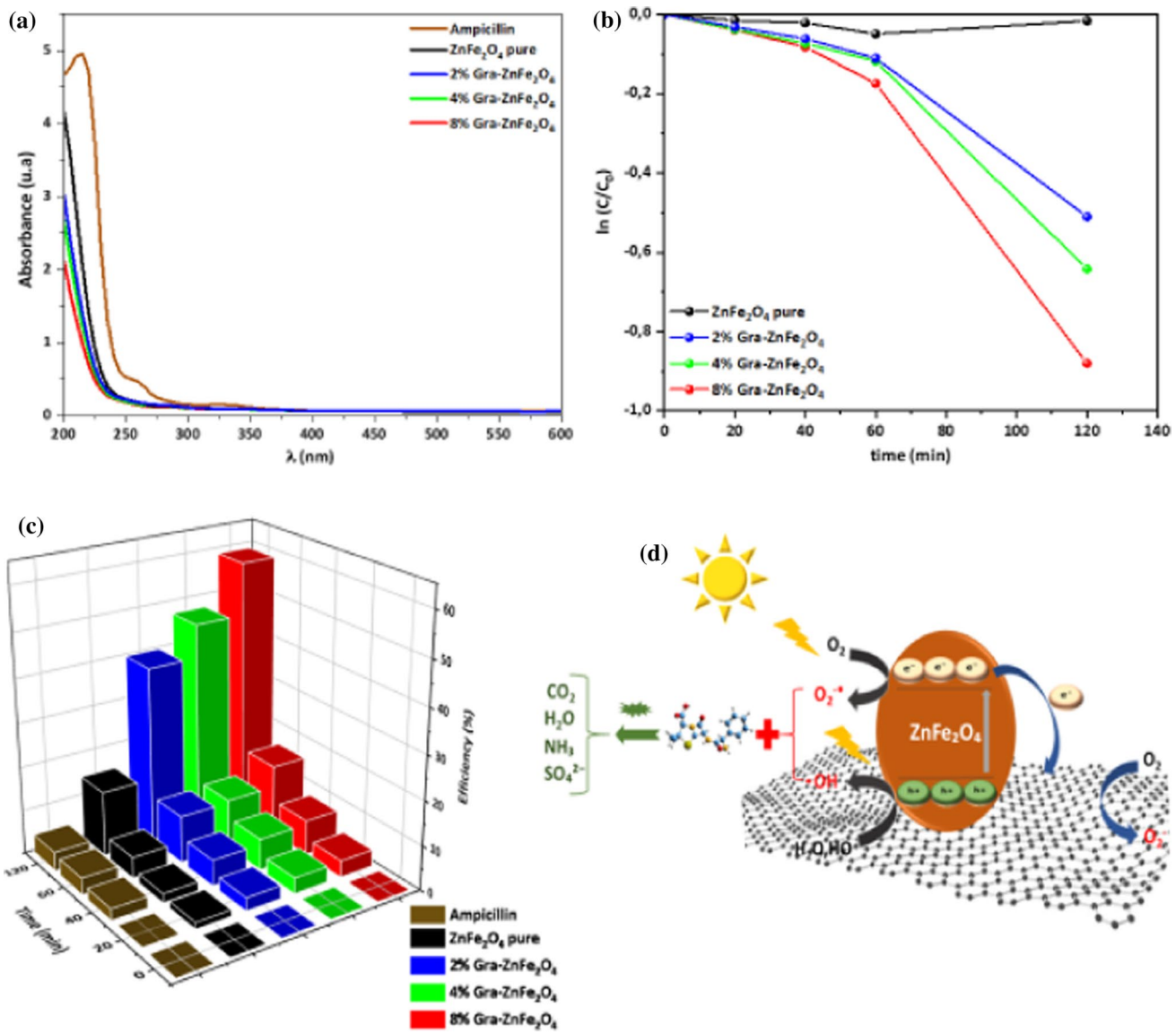

Figure 8 **a** Absorption spectra of pristine $ZnFe_2O_4$ and graphene–$ZnFe_2O_4$ nanocomposites at different graphene loadings (2, 4, and 8 wt%) under visible light irradiation; **b** pseudo first-order kinetics of RhB photodegradation for the same samples; **c** photodegradation efficiency of pristine $ZnFe_2O_4$ and graphene–$ZnFe_2O_4$ nanocomposites at different graphene loadings (2, 4, and 8 wt%) after 2 h of visible light irradiation using thin film photocatalysts, with an initial ampicillin concentration of 10 mg/L; and **d** schematic illustration of the photodegradation mechanism.

our 60% ampicillin degradation in just 2 h using a thin film, under natural sunlight, and without pH adjustment or sacrificial agents demonstrates not only efficiency but also practical scalability. This performance validates the synergistic effect of graphene incorporation, which enhances light harvesting and charge carrier dynamics and supports the potential application of our material in environmentally friendly and solar-driven water purification systems.

While cyclic reusability and post-reaction stability tests were not performed in this study, the immobilized Gra–$ZnFe_2O_4$ thin films inherently provide excellent practical stability and reusability. Unlike powder photocatalysts, which are prone to aggregation, scattering losses and difficult recovery, thin films remain physically robust, easy to handle, and can be reused directly without filtration or material loss. This immobilization ensures that the photocatalyst maintains

its structural integrity and functional performance under sunlight irradiation, highlighting its suitability for water treatment applications [46, 47]. Systematic evaluation of metal oxide photocatalysts indicates that sunlight-induced degradation efficiency varies considerably across different compositions and synthesis approaches during standard 2 h testing. Notably, ZnO prepared through hydrothermal methods exhibited a comparatively low degradation rate of 41% [36].

Photocatalytic degradation pathway of ampicillin

The proposed photocatalytic degradation pathway of ampicillin using graphene–$ZnFe_2O_4$ nanocomposite is schematically presented in Fig. 8d. Photodegradation mechanisms of β-lactam antibiotics have been extensively investigated in recent literature. Notably, the degradation of structurally related compounds such as amoxicillin has been effectively demonstrated using MIL-53(Al)/ZnO composites [48], while the photocatalytic breakdown of ciprofloxacin has been explored employing $NCuTiO_2$/CQD composites [49]. Ampicillin itself has also been the focus of numerous studies, albeit with different photocatalyst systems such as ZnO/polyaniline nanocomposites, which confirmed key oxidative degradation pathways driven by reactive oxygen species [50].

On the basis of the reported mechanisms, the present work outlines a stepwise visible light-induced photocatalytic degradation mechanism of ampicillin mediated by the graphene–$ZnFe_2O_4$ nanocomposite. The incorporation of graphene enhances charge separation and broadens light absorption, thereby promoting the formation of reactive oxygen species that initiate and sustain the oxidative degradation of ampicillin. This proposed mechanism, consistent with prior reports, provides a rational basis for the photocatalytic degradation pathway of ampicillin (AMP) over the $ZnFe_2O_4$/graphene composite. Upon visible light irradiation, $ZnFe_2O_4$ absorbs photons, promoting electrons from the valence band (VB) to the conduction band (CB) and leaving behind holes ($ZnFe_2O_4 + h\nu \rightarrow ZnFe_2O_4\ (e^- + h^+)$). These photogenerated electrons are efficiently transferred to the π-conjugated graphene network due to its high conductivity, which effectively suppresses charge recombination and prolongs carrier lifetime ($ZnFe_2O_4\ (e^- + h^+) + Gra \rightarrow ZnFe_2O_4\ (h^+) + Gra\ (e^-)$). This charge separation enhances the redox reactivity of the photocatalyst surface and initiates a series of oxidative transformations. The transferred electrons reduce dissolved oxygen to form superoxide radicals ($Gra\ (e^-) + O_2 \rightarrow O_2\bullet^- + Gra$), while the photogenerated holes oxidize water or hydroxide ions to yield hydroxyl radicals ($ZnFe_2O_4\ (h^+) + H_2O/OH^- \rightarrow OH\bullet + H^+ + ZnFe_2O_4$). These reactive oxygen species (ROS), namely, $\bullet OH$ and $\bullet O_2^-$, are highly oxidative and play crucial roles in degrading organic pollutants, as previously demonstrated by Noroozi et al. for $NCuTiO_2$/CQD composites in ciprofloxacin degradation and confirmed through radical scavenging experiments in other β-lactam antibiotic studies [50, 51].

AMP molecules adsorb onto the photocatalyst surface via π–π stacking with graphene and hydrogen bonding with Fe–O groups of $ZnFe_2O_4$, facilitating effective interaction with ROS [36]. The first site of attack is the strained β-lactam ring, which undergoes oxidative cleavage initiated by $\bullet OH$ and $\bullet O_2^-$ radicals, forming unstable intermediates—a process widely reported in ZnO-, TiO_2-, and $ZnFe_2O_4$-based systems. After the β-lactam ring opens, AMP degradation proceeds through two dominant oxidative routes. In Pathway A, oxidation of the phenylglycine moiety leads to benzoic acid formation, which is subsequently oxidized to hydroxylated and decarboxylated organic acids (such as acetic and formic acids) before being fully mineralized to CO_2 and H_2O, consistent with GC–MS findings in previous $ZnFe_2O_4$-based studies [36, 52]. In Pathway B, the sulphur-containing thiazolidine ring is oxidatively cleaved to form sulphonic acid derivatives, while the amine group is transformed into nitrogenous species, including NH_4^+ and NO_3^-, through sequential oxidation steps typical of β-lactam degradation processes. With continued visible light irradiation, both pathways converge towards complete mineralization, yielding non-toxic end-products CO_2, H_2O, NH_4^+, and NO_3^- as verified by total organic carbon (TOC) and ion chromatography analyses in comparable photocatalytic studies [53].

The synergistic action of reactive oxygen species generated during photocatalysis ensures the effective mineralization of ampicillin into environmentally benign compounds. In the Gra–$ZnFe_2O_4$ nanocomposite system, Gra presents a pivotal role as an efficient electron mediator, significantly enhancing the generation of these reactive species. This enhancement is achieved through several mechanisms: (i) prolonging the lifetime of photogenerated charge carriers via

rapid electron transfer, (ii) providing additional active sites for radical formation, and (iii) facilitating greater pollutant adsorption due to its large specific surface area. These combined effects highlight the crucial function of Gra in boosting the photocatalytic performance of $ZnFe_2O_4$. This study clearly demonstrates that the incorporation of Gra offers an effective and innovative strategy for enhancing the degradation of persistent pharmaceutical contaminants such as ampicillin, positioning the Gra–$ZnFe_2O_4$ nanocomposite

Conclusion

Zinc ferrite ($ZnFe_2O_4$) and Gra-based nanocomposites were successfully synthesized via the spray pyrolysis method for the photocatalytic degradation of ampicillin. Pristine $ZnFe_2O_4$ has attracted significant interest due to its chemical stability, magnetic recoverability, and visible light responsive band gap. However, its photocatalytic performance is limited by rapid charge recombination. To overcome this, Gra was incorporated as a conductive additive, leveraging its excellent electron mobility and high surface area to enhance charge separation, light absorption, and pollutant adsorption. The incorporation of 8 wt% Gra into $ZnFe_2O_4$ resulted in a reduced band gap from 3.01 to 2.77 eV, facilitating better visible light harvesting. As a result, the nanocomposite exhibited an ampicillin degradation efficiency of 60%, demonstrating its superior photocatalytic performance. The high photocatalytic degradation efficiency is attributed to the reduction in grain size and changes in surface morphology, as confirmed by XRD and AFM analyses. These modifications result in an increased density of grain boundaries, which act as active sites for photocatalytic reactions and facilitate improved charge carrier separation. Overall, this study demonstrates that the incorporation of Gra is a highly effective strategy for enhancing the photocatalytic performance of $ZnFe_2O_4$, establishing the nanocomposite as a promising candidate for sustainable water treatment applications, particularly in the degradation of pharmaceutical contaminants.

Acknowledgements

This work was supported by the Kempe Foundation, the Knut och Alice Wallenberg Foundation (grant number KAW 2016.346), and the ÅFORSK Foundation.

The authors would also like to acknowledge Ca' Foscari University of Venice for the SPIN2019 project, and Mr. Tiziano Finotto from the Department of Molecular Sciences and Nanosystems, Ca' Foscari University of Venice, Italy, for support on the XRD measurement. A.V. acknowledged financial support by the European Union-NextGenerationEU Programme, the National Recovery and Resilience Plan (NRRP), Mission 4 Component 2 Investment 1.1 PRIN 2022 PNRR Ministero dell'Università e della Ricerca (MUR), CUP D53D23019400001, ID P2022RL4TR "All-oxide nanowire plasmonic solar cells (NanoSolar)." Finally, the authors express their gratitude to the Laboratoire de Physique de la Matière Condensée, Faculté des Sciences de Tunis, Université Tunis El Manar, for their continuous support.

Author contributions

Fatma Ezzahra Dhif was responsible for conceptualization, data curation, investigation, methodology, resources, writing—original draft, and writing review. Neila Jebbari and Kassa Belay Ibrahim were involved in the editing and supervision. Alberto Vomiero, Elisa Moretti, and Najoua Turki-Kamoun contributed to funding acquisition and supervision project.

Funding

The Kempe Foundation,the Knut och Alice Wallenberg Foundation,KAW 2016.346,North Atlantic Treaty Organization,project COD. P2022RL4TR,CUP: H53D23009150001

Data availability

The datasets supporting the results of this article are included within the article.

Declarations

Conflict of interest The authors declare that they have no conflict of interest.

Supplementary information Not applicable.

Ethical approval Not applicable.

References

[1] Patel M, Kumar R, Kishor K, Mlsna T, Pittman CU Jr, Mohan D (2019) Pharmaceuticals of emerging concern in aquatic systems: chemistry, occurrence, effects, and removal methods. Chem Rev 119(6):3510–3673

[2] García-Zamora JL, Alonso-Arenas J, Rebollar-Pérez G, Pacheco-Aguirre FM, García-Diaz E, Torres E (2022) Detection of ampicillin based on the fluorescence of a biocatalytic oxidation product. Front Environ Sci 10:1040903

[3] Montoya-Rodríguez DM, Serna-Galvis EA, Ferraro F, Torres-Palma RA (2020) Degradation of the emerging concern pollutant ampicillin in aqueous media by sonochemical advanced oxidation processes-parameters effect, removal of antimicrobial activity and pollutant treatment in hydrolyzed urine. J Environ Manage 261:110224

[4] Rodriguez-Mozaz S, Chamorro S, Marti E, Huerta B, Gros M, Sànchez-Melsió A, Balcázar JL (2015) Occurrence of antibiotics and antibiotic resistance genes in hospital and urban wastewaters and their impact on the receiving river. Water Res 69:234–242

[5] Comninellis C, Kapalka A, Malato S, Parsons SA, Poulios I, Mantzavinos D (2008) Advanced oxidation processes for water treatment: advances and trends for R&d. J Chem Technol Biotechnol Int Res Process, Environ Clean Technol 83(6):769–776

[6] Zhu X, Zhang F, Wang M, Ding J, Sun S, Bao J, Gao C (2014) Facile synthesis, structure and visible light photocatalytic activity of recyclable $ZnFe_2O_4/TiO_2$. Appl Surf Sci 319:83–89

[7] Farahani N, Kelly PJ, West G, Ratova M, Hill C, Vishnyakov V (2013) An investigation into W or Nb or $ZnFe_2O_4$ doped titania nanocomposites deposited from blended powder targets for UV/Visible photocatalysis. Coatings 3(3):153–165

[8] Novoselov KS, Mishchenko A, Carvalho A, Castro Neto AH (2016) 2D materials and van der Waals heterostructures. Science 353(6298):aac9439

[9] Abbas N, Zhang JM, Ikram M, Ibrahim AA, Nazir S, Ali I, Akhtar H (2024) Investigation of structural, electrical, and thermoelectric properties of cobalt-zinc ferrites/graphene nanocomposite. Results Phys 59:107576

[10] Khan NU, Amin N, Khalid MU, Amami M, Un Nabi MA (2024) Tailoring the structural, electrical, dielectric, and magnetic properties of graphene nanoplatelets (GNPs)-incorporated Ni0. 35Zn0. 25Cd0. $4Fe_2O_4$ ferrite composites. Mate Sci Eng B 308:117580

[11] Wang Q, Domen K (2019) Particulate photocatalysts for light-driven water splitting: mechanisms, challenges, and design strategies. Chem Rev 120(2):919–985

[12] Karyaoui M, Jemia DB, Daoudi M, Bardaoui A, Boukhachem A, Amlouk M, Chtourou R (2021) Physical properties of graphene oxide GO-doped ZnO thin films for optoelectronic application. Appl Phys A 127:1–14

[13] Rao TP, Kumar MS (2010) Physical properties of Ga-doped ZnO thin films by spray pyrolysis. J Alloys Compd 506(2):788–793

[14] Guan S, Cheng Y, Hao L, Yoshida H, Tarashima C, Zhan T, Lu Y (2023) Oxygen vacancies induced band gap narrowing for efficient visible-light response in carbon-doped TiO_2. Sci Rep 13(1):14105

[15] Zhang Y, Pan C (2011) TiO_2/graphene composite from thermal reaction of graphene oxide and its photocatalytic activity in visible light. J Mater Sci 46(8):2622–2626

[16] Zhang H, Lv X, Li Y, Wang Y, Li J (2010) P25-graphene composite as a high performance photocatalyst. ACS Nano 4(1):380–386

[17] Kumar V, Kumar N, Das SB, Singh RK, Sarkar K, Kumar M (2021) Sol-gel assisted synthesis and tuning of structural, photoluminescence, magnetic and multiferroic properties by annealing temperature in nanostructured zinc ferrite. Mater Today Proc 47:6242–6248

[18] Waldron RD (1955) Infrared spectra of ferrites. Phys Rev 99(6):1727

[19] Manikandan V, Vanitha A, Kumar ER, Chandrasekaran J (2017) Effect of sintering temperature on structural and dielectric properties of Sn substituted $CuFe_2O_4$ nanoparticles. J Magn Magn Mater 423:250–255

[20] Toksha BG, Shirsath SE, Mane ML, Patange SM, Jadhav SS, Jadhav KM (2011) Autocombustion high-temperature synthesis, structural, and magnetic properties of $CoCrxFe_2$–xO_4 ($0 \leq x \leq 1.0$). Phys Chem C 115(43):20905–20912

[21] Huerta-Aguilar CA, Diaz-Puerto ZJ, Tecuapa-Flores ED, Thangarasu P (2022) Crystal plane impact of $ZnFe_2O_4$–Ag nanoparticles influencing photocatalytic and antibacterial properties: experimental and theoretical studies. ACS Omega 7(38):33985–34001

[22] Rahmani S, Seyed Dorraji MS, Rahmani S, Hajimiri I, Amani-Ghadim AR (2020) Loading GO/$ZnFe_2O_4$/NiO nanocomposite as a hybrid dielectric/magnetic material into polyurethane foam for the induction of radar absorbing properties. J Mater Sci Mater Electron 31(7):5107–5116

[23] Narayan H, Alemu H, Macheli L, Sekota M, Thakurdesai M, Gundu Rao TK (2009) Role of particle size in visible light photocatalysis of Congo Red using TiO_2·[$ZnFe_2O_4$] x nanocomposites. Bull Mater Sci 32(5):499–506

[24] Vidhya S, Subramanian Y, Durgadevi K, Bharath Sabarish VC, Durairajan A, Graça MPF, Gajendiran J, Azad KA, Gokul Raj S, Ramesh Kumar GG, Kishor Kumar J (2025) Synthesis and characterization of a heterogeneous ternary nanocomposite photocatalyst $BiFeO_3$-Graphene-$NaNbO_3$ for the degradation of MB dye disrupting pulmonary organs. Opt Laser Technol 181:111798

[25] Wang J, Li Y, Ling H, Qiu Y, Lou J, Hou X, Bag SP, Wang J, Wu H, Chai G (2019) Significant enhancement of the visible light photocatalytic properties in 3D $BiFeO_3$/graphene composites. Nanomaterials 9(1):65

[26] Han L, Zhou X, Wan L, Deng Y, Zhan S (2014) Synthesis of $ZnFe_2O_4$ nanoplates by succinic acid-assisted hydrothermal route and their photocatalytic degradation of rhodamine B under visible light. J Environ Chem Eng 2(1):123–130

[27] Ikramullah AN, Ali F, Sheikh ZA, Bilal M, Ahmad I (2020) Photocatalytic performance of zinc ferrite magnetic nanostructures for efficient eriochrome black-T degradation from the aqueous environment under unfiltered sunlight. Water Air Soil Pollut 231(2):59

[28] Doiphode V, Vairale P, Sharma V, Waghmare A, Punde A, Shinde P, Jadkar S (2021) Solution-processed electrochemical synthesis of $ZnFe_2O_4$ photoanode for photoelectrochemical water splitting. J Solid-State Electrochem 25(6):1835–1846

[29] Renuka L, Anantharaju KS, Sharma SC, Vidya YS, Nagaswarupa HP, Prashantha SC, Nagabhushana H (2018) Synthesis of $ZnFe_2O_4$ nanoparticle by combustion and sol gel methods and their structural, photoluminescence and photocatalytic performance. Mater Today Proc 5(10):20819–20826

[30] Kombaiah K, Vijaya JJ, Kennedy LJ, Bououdina M (2016) Studies on the microwave assisted and conventional combustion synthesis of *Hibiscus rosa-sinensis* plant extract based $ZnFe_2O_4$ nanoparticles and their optical and magnetic properties. Ceram Int 42(2):2741–2749

[31] Behera A, Kandi D, Majhi SM, Martha S, Parida K (2018) Facile synthesis of $ZnFe_2O_4$ photocatalysts for decolourization of organic dyes under solar irradiation. Beilstein J Nanotechnol 9(1):436–446

[32] Al-Musawi TJ, Rajiv P, Mengelizadeh N, Arghavan FS, Balarak D (2021) Photocatalytic efficiency of $CuNiFe_2O_4$ nanoparticles loaded on multi-walled carbon nanotubes as a novel photocatalyst for ampicillin degradation. J Mol Liq 337:116470

[33] Mirikaram N, Perez-Molina A, Morales-Torres S, Salemi A, Maldonado-Hódar FJ, Pastrana-Martinez LM (2021) Photocatalytic performance of ZnO-graphene oxide composites towards the degradation of vanillic acid under solar radiation and visible-LED. Nanomaterials 11(6):1576

[34] Liu J, Chen KY, Wang J, Du M, Gao ZY, Song CX (2020) Preparation and photocatalytic properties of N-doped Graphene/TiO_2 composites. J Chem 2020(1):2928189

[35] Li H, Wei J, Qian Y, Zhang J, Yu J, Wang G, Xu G (2014) Effects of the graphene content and the treatment temperature on the supercapacitive properties of VOx/graphene nanocomposites. Colloids Surf A Physicochem Eng Asp 449:148–156

[36] Nosrati R, Olad A, Maramifar R (2012) Degradation of ampicillin antibiotic in aqueous solution by ZnO/polyaniline nanocomposite as photocatalyst under sunlight irradiation. Environ Sci Pollut Res 19(6):2291–2299

[37] Ghribi F, Sehailia M, Aoudjit L, Touahra F, Zioui D, Boumechhour A, Benmaamar Z (2020) Solar-light promoted photodegradation of metronidazole over ZnO-$ZnAl_2O_4$ heterojunction derived from 2D-layered double hydroxide structure. J Photochem Photobiol A Chem 397:112510

[38] Verma M, Haritash AK (2020) Photocatalytic degradation of Amoxicillin in pharmaceutical wastewater: a potential tool to manage residual antibiotics. Environ Technol Innov 20:101072

[39] Ramos RMB, Paludo LC, Monteiro PI, da Rocha LVM, de Moraes CV, Santos OO, Dantas TLP (2023) Amoxicillin degradation by iron photonanocatalyst synthetized by green route using pumpkin (Tetsukabuto) peel extract. Talanta 260:124658

[40] Mashentseva AA, Nurpeisova DT, Barsbay M (2024) Effect of copper doping on the photocatalytic performance of Ni_2O_3@ PC membrane composites in norfloxacin degradation. RSC Adv 14(7):4424–4435

[41] Gherasim C, Pascariu P, Asandulesa M, Dobromir M, Doroftei F, Fifere N, Airinei A (2022) Copper oxide nanostructures: preparation, structural, dielectric, and catalytic properties. Ceram Int 48(17):25556–25568

[42] Wu Y, Ji H, Liu Q, Sun Z, Li P, Ding P, Chen S (2022) Visible light photocatalytic degradation of sulfanilamide enhanced by Mo doping of BiOBr nanoflowers. J Hazard Mater 424:127563

[43] Dong S, Cui L, Liu C, Zhang F, Li K, Xia L, Sun J (2019) Fabrication of 3D ultra-light graphene aerogel/Bi_2WO_6 composite with excellent photocatalytic performance: a promising photocatalyst for water purification. J Taiwan Inst Chem Eng 97:288–296

[44] Dong S, Ding X, Guo T, Yue X, Han X, Sun J (2017) Self-assembled hollow sphere-shaped Bi_2WO_6/RGO composites for efficient sunlight-driven photocatalytic degradation of organic pollutants. Chem Eng J 316:778–789

[45] Tzeng TW, Wang SL, Chen CC, Tan CC, Liu YT, Chen TY, Hung JT (2016) Photolysis and photocatalytic decomposition of sulfamethazine antibiotics in an aqueous solution with TiO_2. RSC Adv 6(73):69301–69310

[46] Pedanekar RS, Shaikh SK, Rajpure KY (2020) Thin film photocatalysis for environmental remediation: a status review. Curr Appl Phys 20(8):931–952

[47] Covei M, Bogatu C, Gheorghita S, Duta A, Stroescu H, Nicolescu M, Gartner M (2023) Influence of the deposition parameters on the properties of TiO_2 thin films on spherical substrates. Materials 16(14):4899

[48] Fawzy A, Mahanna H, Mossad M (2022) Effective photocatalytic degradation of amoxicillin using MIL-53 (Al)/ZnO composite. Environ Sci Pollut Res Int 29(45):68532–68546

[49] Noroozi R, Gholami M, Oskoei V, Hesami Arani M, Mousavifard SA, Nguyen Le B, Fattahi M (2023) Fabrication of new composite NCuTiO$_2$/CQD for photocatalytic degradation of ciprofloxacin and pharmaceutical wastewater treatment: degradation pathway, toxicity assessment. Sci Rep 13(1):16287

[50] Olad A, Nosrati R (2015) Use of response surface methodology for optimization of the photocatalytic degradation of ampicillin by ZnO/polyaniline nanocomposite. Res Chem Intermed 41(3):1351–1363

[51] Rasheed-Adeleke AA, Olatunde OC, Seheri NH, Oyewo OA, Ferjani H, Onwudiwe DC (2025) Synthesis and photocatalytic performance of $ZnFe_2O_4$ on the degradation of tetracycline in water. Appl Phys A Mater Sci Process 131(8):1–9

[52] Truong HB, Huy BT, Ray SK, Gyawali G, Lee YI, Cho J, Hur J (2022) Magnetic visible-light activated photocatalyst $ZnFe_2O_4/BiVO_4/g\text{-}C_3N_4$ for decomposition of antibiotic lomefloxacin: photocatalytic mechanism, degradation pathway, and toxicity assessment. Chemosphere 299:134320

[53] Alfred MO, Olorunnisola CG, Oyetunde TT, Dare P, Vilela RR, de Camargo A, Unuabonah EI (2022) Sunlight-driven photocatalytic mineralization of antibiotic chemicals and selected enteric bacteria in water via zinc tungstate-imprinted kaolinite. Green Chem Lett Rev 15(3):705–723